Relative interfacial cleavage energetics of protein complexes revealed by surface collisions

Sophie R. Harvey[a,b,1], Justin T. Seffernick[a,b,1], Royston S. Quintyn[a,2], Yang Song[a,3], Yue Ju[a,4], Jing Yan[a,5], Aniruddha N. Sahasrabuddhe[a,6], Andrew Norris[a], Mowei Zhou[a,7], Edward J. Behrman[a], Steffen Lindert[a,b,8], and Vicki H. Wysocki[a,b,8]

[a]Department of Chemistry and Biochemistry, The Ohio State University, Columbus, OH 43210; and [b]Resource for Native Mass Spectrometry Guided Structural Biology, The Ohio State University, Columbus, OH 43210

Edited by Carol V. Robinson, University of Oxford, Oxford, United Kingdom, and approved March 1, 2019 (received for review October 12, 2018)

To fulfill their biological functions, proteins must interact with their specific binding partners and often function as large assemblies composed of multiple proteins or proteins plus other biomolecules. Structural characterization of these complexes, including identification of all binding partners, their relative binding affinities, and complex topology, is integral for understanding function. Understanding how proteins assemble and how subunits in a complex interact is a cornerstone of structural biology. Here we report a native mass spectrometry (MS)-based method to characterize subunit interactions in globular protein complexes. We demonstrate that dissociation of protein complexes by surface collisions, at the lower end of the typical surface-induced dissociation (SID) collision energy range, consistently cleaves the weakest protein:protein interfaces, producing products that are reflective of the known structure. We present here combined results for multiple complexes as a training set, two validation cases, and four computational models. We show that SID appearance energies can be predicted from structures via a computationally derived expression containing three terms (number of residues in a given interface, unsatisfied hydrogen bonds, and a rigidity factor).

protein complex | native mass spectrometry | protein interactions | structural biology | surface-induced dissociation

Native mass spectrometry (MS) has emerged as a powerful structural biology tool. By using "soft" ionization techniques such as nanoelectrospray ionization, noncovalent interactions can be retained, enabling the study of intact protein:protein, protein:ligand, and protein:RNA complexes in the gas phase (1–4). Native MS overcomes many of the barriers associated with traditional protein characterization methods; it requires low sample volumes (3–10 μL) and micromolar or lower concentrations, while also having a broad mass range for analysis, allowing study of small monomeric proteins up to large megadalton assemblies (1, 5).

Typical MS experiments to study subunit interactions of protein complexes involve first preparing the sample in an aqueous solution at near neutral pH, typically 100–200 mM ammonium acetate. The complex is then introduced intact into the mass spectrometer to measure the mass of the native complex. To obtain subunit connectivity information on the sample, the complex can be disrupted in solution, typically either with small volumes of organic solvent or through alteration of the ionic strength; this destabilizes the protein:protein interfaces and allows measurement of stable subcomplexes (6, 7). This approach, however, targets all species present in solution and can therefore be problematic for heterogeneous samples where it may not be possible to decipher which subcomplex came from which precursor. Alternatively, the complex can be isolated and then dissociated in the gas phase. The most commonly used dissociation method for such studies is collision-induced dissociation (CID). In CID protein ions are accelerated into a bath gas with which they undergo multiple collisions. CID proceeds via an unfolding mechanism and therefore typically produces an unfolded monomer (which typically carries half the charge of the precursor ion) and the corresponding $(n - 1)$ multimer (which retains the other half of the charge) (8–10). CID is a very effective tool for confirming stoichiometry; however, due to the unfolding mechanism it often provides limited information on assembly.

An alternative activation/dissociation method for protein complexes is surface-induced dissociation (SID). In SID ions are accelerated toward and collide against a surface. This is a fast, high-energy deposition process which enables faster, more structurally informative dissociation pathways to outcompete the slower multistep activation unfolding and rearrangement pathways typically observed for CID (11, 12). We have previously shown that SID produces fragments in which the charge is more symmetrically partitioned than it is in CID and that products can remain compact (13–15). In addition, we have demonstrated that SID disassembly pathways are consistent with the known protein assembly pathways and hence can provide structural information on known and unknown structures (16–18). To expand upon

Significance

There is a large gap between the number of protein complex structures currently solved and the number of functionally relevant structures. Mass spectrometry-based approaches for biomacromolecule structural characterization are growing, are beginning to fill critical gaps, and complement other structural biology tools. We have shown for several examples that collision of protein complex ions with a surface yields products that are reflective of substructure. We present here a computational model that predicts the relative appearance energy at which a globular protein complex dissociates. This appearance energy prediction can provide structural information when a high-resolution structure has not or cannot be obtained and in the future has potential to be used to select the best-fit candidate computational models, dramatically increasing the structural information obtained.

Author contributions: S.R.H., M.Z., S.L., and V.H.W. designed research; S.R.H., J.T.S., R.S.Q., Y.S., Y.J., J.Y., A.N.S., A.N., M.Z., and E.J.B. performed research; E.J.B. contributed new reagents/analytic tools; S.R.H., J.T.S., R.S.Q., Y.S., Y.J., J.Y., A.N.S., A.N., and S.L. analyzed data; and S.R.H. and V.H.W. wrote the paper.

The authors declare no conflict of interest.

This article is a PNAS Direct Submission.

[1]S.R.H. and J.T.S. contributed equally to this work.

[2]Present address: Chromatography and Mass-Spectrometry Division, Thermo Scientific, West Palm Beach, FL 33407.

[3]Present address: Attribute Sciences, Amgen Massachusetts, Cambridge, MA 02142.

[4]Present address: Pharma/BioPharma Business Group, Bruker Daltonis, San Jose, CA 95134.

[5]Present address: Pivotal Attribute Science, Process Development, Amgen Inc., Thousand Oaks, CA 91320.

[6]Present address: Discovery Technologies, Amgen, Thousand Oaks, CA, 91320.

[7]Present address: Environmental Molecular Sciences Laboratory, Pacific Northwest National Laboratory, Richland, WA 99354.

[8]To whom correspondence may be addressed. Email: lindert.1@osu.edu or wysocki.11@osu.edu.

This article contains supporting information online at www.pnas.org/lookup/suppl/doi:10.1073/pnas.1817632116/-/DCSupplemental.

Published online April 3, 2019.

these previous studies and to more fully characterize SID and its utility in structural biology studies, we chose a set of globular protein complexes with different oligomeric orders and of known structure to determine whether SID consistently produces subcomplexes reflective of the solved structure. We coupled our experimental studies with computational approaches to discern which structural factors of the protein complex determine the appearance energy for fragmentation. In future studies this would then allow the SID pattern and energy requirements to predict the overall topology of a complex of unknown structure and to position the complex in the periodic table of protein complexes (19).

Results and Discussion

SID Patterns for Oligomers of Different Structures. All protein complexes (Fig. 1) were studied under native-like conditions. Complexes were studied under charge-reducing conditions, afforded by preparing the protein in ammonium acetate and triethylammonium acetate, to keep the proteins more compact and native-like (20). Under these conditions, CID proceeds via the typical unfolding mechanism, producing unfolded, highly charged monomers, providing no direct information on subunit connectivities (*SI Appendix*, Figs. S1–S5, *Left*). In contrast, SID produces a wide range of different subcomplexes.

Dimers can only fragment to monomers or fragment covalently along the backbone, and we first consider the homodimers triose phosphate isomerase and phosphorylase B (*SI Appendix*, Fig. S1). The main differences in CID and SID for dimers are that the monomers produced by CID often show the typical asymmetric charge partitioning while SID typically produces symmetrically charged species. As the oligomeric order of protein complexes increases, the range of products that can be produced also increases. We next considered the homotetrameric proteins streptavidin, neutravidin, and pyruvate kinase, for which low-energy SID primarily produces dimers (*SI Appendix*, Fig. S2 *D–F*) and in some cases lower-intensity monomers (in contrast to forming primarily monomers by CID; *SI Appendix*, Fig. S2 *A–C*). These tetramers are all dimers of dimers and have D_2 symmetry. We performed preliminary structural analysis using Proteins, Interfaces, Structures, and Assemblies (PISA) interfacial prediction (21) (Fig. 1). PISA can predict the interfacial area, the number of salt bridges, and the number of hydrogen bonds at the interface between protein subunits. PISA reveals that the interface between the two monomers forming the dimer (interface A) is much stronger than the other two interfaces present (B and C) for these three homotetrameric complexes. Therefore, the theoretically most favorable dissociation pathway is dissociation from tetramers to dimers, based upon cleaving the smallest total interfacial area (IA) and correspondingly cleaving fewer predicted intermolecular interactions, salt bridges (SBs), and hydrogen bonds (HBs). For example, for streptavidin to produce dimers (cleaving two C and two B interfaces) an IA of 1,176 Å^2 would be cleaved whereas to produce a monomer and a trimer (cleaving one A, one C, and one B interface) an IA of 2,139 Å^2 would be cleaved (16). The dissociation pathway to produce dimers is, therefore, predicted to be more favorable (by ~1,000 Å^2) and is consistent with our SID results.

In contrast, for the D_2 tetramers transthyretin, Con A, d-sialic acid aldolase, and hemoglobin, PISA predicts that the three interfaces present in these complexes are more similar, with respect to interfacial area, than in the previous set of tetramers. Therefore, the IAs that would have to be broken to produce the different products (namely dimer + dimer vs. monomer + trimer) are more similar than in the previous set of tetramers. For example, for transthyretin to dissociate from the tetramer to produce dimers (cleaving two C and two B interfaces) a total IA of 1,398 Å^2 has to be cleaved whereas to produce a monomer and a trimer (cleaving one A, one C, and one B interface) a total interfacial area of 1,573 Å^2 would be cleaved. These two dissociation pathways are closer in relative interfacial area cleaved (differing by only 175 Å^2), and hence both might be expected to occur with low-energy SID. Indeed, for transthyretin, Con A, d-sialic acid aldolase, and hemoglobin both pathways (production of dimers and production of monomer and trimer) are observed in the low-energy SID spectrum (*SI Appendix*, Fig. S3 *E–H*). A significantly higher proportion of monomer is observed here (*SI Appendix*, Fig. S3 *E–H*) compared with the previous tetramers (*SI Appendix*, Fig. S2 *D–F*).

Finally, we considered the heterotetramer tryptophan synthase, which is composed of a β dimer flanked by two α subunits in a linear arrangement. PISA interfacial prediction highlights that tryptophan synthase has a stronger interface between the two β subunits than between the α and β subunits. Correspondingly, in low-energy SID the formation of an α monomer and the complementary ββα trimer is observed (22).

We next present the cyclic pentamers cholera toxin B, C-reactive protein, and serum amyloid P, all of which have equal interfaces between subunits (Fig. 1). With equal interfaces between all subunits it is predicted that cleavage will occur at any two interfaces, forming both monomer and tetramer, plus dimer and trimer. The PISA interfacial predictions are entirely consistent with experimental SID (*SI Appendix*, Fig. S4 *D–F*), demonstrating that SID can produce subcomplexes consistent with the solved structure for complexes of different oligomeric orders and with varied subunit arrangements.

To further expand this approach we also examined homohexameric complexes. Glutamate dehydrogenase (GDH) and urease are both dimers of trimers, which have strong A interfaces between the monomers forming the trimer and weaker B and C interfaces, bringing the two trimers together to form the hexamer. For both of these hexamers, cleaving the lowest interfacial area would produce trimers as observed experimentally by SID (*SI Appendix*, Fig. S5*C*, bovine GDH) as previously reported (23). We also considered insulin which can be considered to be a trimer of dimers; it has more equal interfaces between the subunits and hence is predicted to dissociate to dimer and tetramer, monomer and pentamer, plus trimer and trimer. Experimentally all pathways are indeed observed in low-energy SID (*SI Appendix*, Fig. S5*D*). This set of hexamers demonstrates that SID can distinguish between different subunit connectivities and provide insight into structure.

Finally, we studied the dodecamer glutamine synthetase, which is composed of two stacked hexameric rings. PISA interfacial prediction identifies the strongest interface as an interring interface (*SI Appendix*, Fig. S6*A*), followed by an intraring interface (*SI Appendix*, Fig. S6*B*) and another weaker interring interface (*SI Appendix*, Fig. S6*C*). Producing dimer and undecamer, tetramer and octamer, and two hexamers involves breaking the lowest IA (6,494 Å^2) with only a slightly higher IA having to be broken to produce the monomer and 11-mer (6,958 Å^2) (*SI Appendix*, Table S1). Interfacial prediction is again consistent with our experimental SID results (*SI Appendix*, Fig. S7). For all complexes studied here, from tetramer to dodecamer, SID cleaves the weakest protein:protein interfaces, producing the products predicted from the interfacial analysis.

Computational Modeling to Predict SID Appearance Energies. We have demonstrated that the subcomplexes produced from SID of a range of different complexes with different known oligomeric states and connectivities can be predicted from the known structure of the complex. This is consistent with our previous work where we have used SID subcomplex products to predict connectivity for complexes of unknown structure (17). The utility of SID as a structural biology tool could be increased if the appearance energy required to produce the subcomplex could also be related to the structure. The potential to predict SID appearance energies (AEs), defined here as 10% fragmentation, based on structural features of protein:protein interfaces (PPIs) was also investigated. For this analysis, initially a subset of seven globular complexes was chosen that have a complete complex structure deposited in the Protein Data Bank as opposed to a structure assembled in PISA. SID energy-resolved MS (ERMS) plots were generated for each protein complex studied (*SI Appendix*, Figs.

Oligomer	Interfacial Analysis: interface area (IA)/ Å², salt bridges (SB), hydrogen bonds (HB)			Subunits produced Corresponding interfacial area broken on dissociation					Expected product	Observed Product
	**Triose Phosphate isomerase (PDB 8TIM)**									
	IA:1607 SB:8 HB: 26			M: 1607					2M	2M
	Phosphorylase B, 196 kDa (PDB 1ABB)									
	IA:2498 **SB: 14.5 HB:38**			M: 2498					2M	2M
	Streptavidin, 53 kDa (PDB 1SWB)									
	A: IA:1551 SB:2 HB: 12.5	B: IA:415 SB:0 HB:2	C: IA:173 SB:0 HB:0.5	**D(I-IV + III-II): 1176**	D(I-II + III-IV): 3448	D(I-III + IV-II): 3932	M + T: 2139	4M: 4278	2D	2D
	Neutravidin, 59 kDa (PDB 1VYO)									
	A: IA:1889 SB:6 HB:28.5	B: IA:550 SB:0 HB:5	C: IA:144 SB:0 HB:5	**D(I-IV + III-II): 1388**	D(I-II + III-IV): 4066	D(I-III + IV-II): 4878	M + T: 2593	4M: 5166	2D	2D
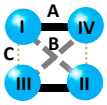	Pyruvate Kinase 237 kDa (PDB 1AQF)									
	A: IA: 2733 SB:4 HB:14.5	B: IA:1270 SB:2 HB:10	C: IA:37 SB:0 HB:0	**D(I-IV + III-II): 2614**	D(I-II + III-IV): 5540	D(I-III + IV-II): 8066	M+T: 4040	4M: 8080	2D	2D
	Concanavalin A, 103 kDa (PDB 3CNA)									
	A: IA: 1085 SB:0 HB:10	B: IA: 982 SB:6 HB:2	C: n/a SB: HB:	**D(I-IV + III-II): 1964**	D(I-II + III-IV): 2170	D(I-III + IV-II): n/a	M+T: 2067	4M: 4134	2D, M+T	2D, M+T
	Transthyretin, 55 kDa (PDB 1F41)									
	A: IA:874 SB:0 HB:16	B: IA:379 SB:0 HB:2	C: IA:320 SB:0 HB:3	**D(I-IV + III-II): 1398**	D(I-II + III-IV): 2506	D(I-III + IV-II): 2388	M+T: 1573	4M: 3146	2D, M+T	2D, M+T
	D-Sialic acid aldolase 135 kDa (PDB 3LBM)									
	A: IA: 1148 SB:3.5 HB:12	B: IA:998 SB:6 HB: 16.5	C: IA:401 SB: 2 HB:3	**D(I-IV + III-II): 2798**	D(I-II + III- IV): 3098	D(I-III + IV-II): 4292	**M+T: 2547**	4M: 5094	2D, M+T	2D, M+T
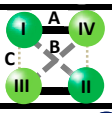	**Hemoglobin, 65 kDa (PDB 1GZX)**									
	A: 846 SB:0 HB:7	B: 663 SB:0.5 HB:5	C: 258 SB:1 HB:2	**D(I-IV + III-II): 1842**	D(I-II + III- IV):2208	D(I-III + IV-II): 3018	**M + T: 1767**	4M: 3534	2D, M+T	2D, M+T
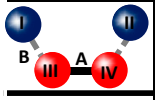	Tryptophan Synthase, 144 kDa (PDB 1WBJ)									
	A: 1624 SB:4 HB:18	B: 1362 SB:1 HB:19		D(I-III + IV-II): 1624	**M+T (I + III- IV-II): 1362**	D+ 2M (III-IV + I +II): 2724		4M: 4610	M+T	M+T
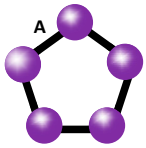	**Cholera toxin B, 58 kDa (PDB 1FGB)**									
	A: 1227 SB:3 HB:12.6			**M + Q: 2454**	**D + T: 2454**	5M: 135			M+Q, D+T	M+Q, D+T
	C-reactive protein, 115 kDa (PDB 1GNH)									
	A: 666 SB:4.4 HB:2.4			**M + Q: 1332**	**D + T: 1332**	5M: 330			M+Q, D+T	M+Q, D+T
	Serum amyloid P, 125 kDa (PDB 1SAC)									
	A: 735 SB: 2.2HB:5			**M + Q: 1470**	**D + T: 1470**	5M: 675			M+Q, D+T	M+Q, D+T
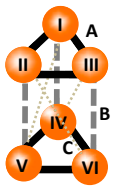	**Bovine glutamate dehydrogenase , 336 kDa (PDB 3MVO)**									
	A: IA: 1691 SB:0.3 HB:10	B: IA: 991 SB:2 HB:9	C: IA:298 SB:0 HB:0	**2T(I-II-II + IV-V- VI): 3867**	3D(I-IV+ II-V + III- VI): 1040	D (I-IV) + Q: 7360	D (I-II) + Q: 5960	M + P: 4671	6M: 14013	2T	2T
	Urease, 549 kDa (PDB 3LA4)									
	A: IA:4888 SB:13.8 HB:53.7	B: IA: 749 SB:0 HB:2	C: IA:228 SB:0 HB:0	**2T(I-II-II + IV-V- VI): 2931**	3D(I-IV+ II-V+III- VI): 30012	D (I-IV) + Q: 20008	D (I-II) + Q: 11730	M+ P: 10753	6M: 32259	2T	2T
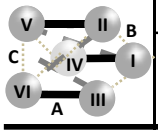	Insulin, 35 kDa (PDB 2AIY)									
	A: IA: 1796 SB:4 HB:16.3	B: IA:458 SB:1.2 HB:5.3	C: IA:844 SB:0 HB:14	**2T (II-V- VI + I-III- VI): 4014**	3D (I- IV+II- V,+III-VI): 5280	**D (I-IV) + Q: 3520**	D (I-II) + Q: 6276	**M + P: 3556**	6M: 10668	D+Q, M+P	D+Q, M+P

Fig. 1. Interfacial information for the proteins studied, in addition to the predicted and observed SID products. Proteins highlighted in boldface type were used for the computational modeling. Only proteins for which a crystal or NMR structure for the complex exists (as opposed to a PISA predicted structure) were used for modeling. Interfacial analysis was performed with PISA analysis and is reported in the form of interface area (IA)/Å^2, salt bridges (SB), and hydrogen bonds (HB). The largest interface in each complex is represented by a solid black line, the second largest interface in each complex is represented by a gray dashed line, and the smallest interface is represented by a gray dotted line. For products: D, dimer; H, hexamer; M, monomer; P, pentamer; Q, tetramer; T, trimer. For representative SID spectra see *SI Appendix*. For phosphorylase B the crystal structure is a tetramer; dimer interfaces were predicted from PISA.

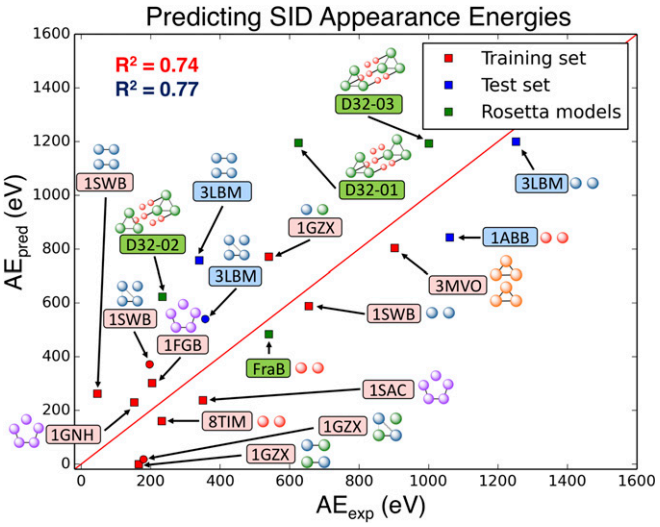

Fig. 2. Optimized model for predicting SID AE. Eq. **1** contains the following parameters: NR, number of residues at the interface; RF, rigidity factor; UHB, number of unsatisfied hydrogen bonds at the surface. There is a strong correlation between predicted and experimental AE for the training set (R^2 = 0.74, red), and the test set (R^2 = 0.77, blue). Tetramers dissociating to monomer–trimer are shown as red circles. Four proteins for which Rosetta models exist were also tested (green) and also show good correlation [three computationally designed dodecamers (D32-01 to -03) (27) and *Salmonella* FraB deglycase (FraB)]. A simplest model structure of each complex is included to show interface cleavages associated with low AE. PDB codes for each protein in the training and test sets are given in red rounded rectangles.

S8–S10). For the tetramers (1SWB, 1GZX, 3LBM), we were able to extract AEs for multiple interfaces. In addition to the dimer–dimer interfaces, we also calculated an AE for the monomer–monomer interface of the dissociated dimers. For example, 1SWB (homotetramer) first dissociated into dimers, resulting in an appearance energy of 184 eV for the dimer–dimer interface. At higher acceleration energies, 1SWB dissociated into monomers, which could have appeared from the tetramer directly (resulting in monomer + trimer) or from the dimers. To calculate the appearance energy from the dimer complex, we subtracted the trimer curve from the monomer curve, which indicates monomers that dissociated from dimers since the number of monomers from trimers should be equal to the number of trimers, resulting in an appearance energy of 655 eV for the interface in the dimer subcomplex. We used similar methodology to calculate appearance energies of subcomplexes for the remaining tetramers. For the SID dataset, Rosetta's InterfaceAnalyzer (24) was used to calculate several interface features (such as IA, HB, SB, etc.) to analyze correlation to SID AE. While some of the calculated interface features individually showed a correlation to AE (*SI Appendix*, Fig. S11) (number of interface residues, R^2 = 0.52; interface surface area, R^2 = 0.40; interface hydrophobic surface area, R^2 = 0.32; Rosetta interface ΔG, R^2 = 0.17), a model that combined several interfacial features allowed more accurate AE prediction (Fig. 2). We also considered correlation to molecular weight only, which showed poorer correlation than the model combining several interfacial features (*SI Appendix*, Fig. S12). The model vastly improved when information about the rigidity of individual subunits was included, using a metric called the rigidity factor (RF). The RF is based on the density of intrasubunit SB, HB, and disulfide bonds. We hypothesize that this term accounts for any partial unfolding upon surface collision, reflecting entropic contributions. Although SID typically produces compact species, with compact collision cross-sections measured from ion mobility, and with ligand retention (25, 26), it is possible that flexible species can partially unfold or rearrange as the energy is redistributed throughout the system after surface collision and before dissociation. The best predictive model for estimating appearance energies from structure, using the computed parameters and shown in Eq. **1**, contained nonzero weights (w) for the number of interacting residues (NRs) at the interface, the number of unsatisfied HBs (UHBs) at the interface, and the RF. The weights were optimized to maximize prediction power, i.e., minimizing χ^2 between predicted and experimental values. The model suggests that larger interfaces (higher NR) have higher AE, interfaces with a larger number of UHBs have lower AE, and interfaces with more rigid subunits (RF) have lower AE. Fig. 2 shows the strong correlation (R^2 = 0.74) between the predicted AE (AE_{pred}) and the experimental AE (AE_{exp}) for the training set, shown in red. Because of concern about error associated with calculation of the AE for secondary dissociation of dimers to monomers (subtraction of the trimer curve, with trimer possibly discriminated against experimentally), we also extracted the trimer–monomer interface AEs by using the 10% monomer onset and plotted those points on the plot in Fig. 2 (red circles) and found that they fit well to the model, changing the R^2 to 0.70.

$$AE_{pred} = w_{NR}NR - w_{UHB}UHB - w_{RF}RF = 22.96 * NR - 126.62 * UHB - 517.20 * RF. \quad [1]$$

The majority of the complexes chosen to build this model had similar experimental and predicted AE but there was a clear lack of model complexes with AE > 1,000 eV. To further validate the model and expand the approach, we selected two additional protein complexes that have solved structures and that the model predicted to have higher AE. We found that the experimental AE and predicted AE have good agreement using the model developed with the training set (two known validation complexes shown in blue in Fig. 2), with the R^2 improving slightly after inclusion of the additional complexes (R^2 = 0.77). Finally, we further tested this approach for complexes with no experimentally determined, solved structure. We chose three computationally designed dodecamers, which have been previously studied using SID (27), and a protein complex which has a computational homology model. The predicted and experimental AEs for the four Rosetta models (shown in green in Fig. 2) show good correlation using this approach. The correlation for these models is not as high as in the training and validation sets, which is expected, given that we do not have solved structures for these complexes and there may be some variations in interface strength between the computational or homology model and the experimental structure. However, a greater correlation between experimental and predicted AE is achieved when using this model as opposed to using molecular weight alone. It is important to note that all experiments were performed using charge-reducing conditions, gentle instrumental settings, and no disruptive organic solution additives to keep the complexes compact and native-like. The correlation shown in Fig. 2 suggests that the native conditions chosen maintain the interfaces of these complexes intact until SID occurs. For a set of dimers not included here, we have seen that AE varies very little, for SID of normal and reduced charge species, suggesting that the interfaces remain intact in those cases and that any change in charging is the result of changes on noninterfacial regions of the complex. If complexes are activated or denatured (e.g., through the addition of organic solvents), the interfaces could be disrupted, affecting the relationship between experimental and predicted appearance energy. We have previously reported that AE can change if structure is disrupted (e.g., by in-source CID) (28). The form of Eq. **1** may also change when not just appearance energy, but the ability to select among candidate structural models is the goal.

Conclusions

We have demonstrated that low-energy SID consistently cleaves the weakest interfaces in globular protein complexes in a manner

concordant with their known structures, under charge-reducing conditions. In cases where the difference in total cleaved interfacial area for two competing pathways is small, both pathways are detected near the onset. Furthermore, we have constructed a model that can predict the AE for subcomplex formation based on protein complex structural features. The potential to utilize subunit interactions, connectivities, and agreement between experimental and predicted appearance energies for the selection of candidate structural models in a direct MS/MS experiment is promising with the potential to enhance future MS-based structural biology approaches.

Materials and Methods

Synthesis of the Perfluorodecylethanethiol (FC_{12}). The $CF_3(CF_2)_9CH_2CH_2SH$ for self-assembled monolayer surfaces was synthesized following multiple significant improvements to a previously published protocol (29). The material was characterized by melting-point analysis, IR spectroscopy, and NMR. Full details on the synthesis and characterization can be found in the *SI Appendix*

Preparation of the Self-Assembled Monolayer Surfaces. A 17-mm × 13-mm × 0.5-mm gold surface slide, 1,000 Å of Au on 50 Å of Ti on glass (EMF Corp.), was cleaned for 15 min in a UV cleaner (Model 135500; Boekel Scientific). The cleaned surface was then incubated in ∼3 mL of 1-mM solution of FC_{12} in ethanol for at least 12 h in the dark. Following incubation, the surface was cleaned by sonicating in ∼3 mL of ethanol for 1 min; this process was repeated six times with fresh aliquots of ethanol.

Modification of Synapt G2 and G2S for Surface-Induced Dissociation. All SID experiments were performed on in-house–modified Synapt G2 or G2S instruments (Waters). The instrument was modified as previously described (13); however, in this case the SID device was placed before the ion mobility (IM) cell and hence referred to as Trap-SID. In brief, the Trap t-wave region was truncated by 3 cm without damaging critical electrical parts to accommodate the SID device which was voluntarily machined and provided by Waters Corporation, as a copy of the previous Wysocki group design but with improved mounting brackets. In the current design, the connections for the 10 lenses in the SID device (*SI Appendix*, Fig. S13) are supplied through a Fischer connection through a modified Triwave chamber cover and supplied using an external power supply (Ardara Technologies).

Surface-Induced Dissociation Ion Mobility-Mass Spectrometry. All proteins were introduced into the mass spectrometer using nanoelectrospray ionization in positive ionization mode. Nanoelectrospray tips were made in house using thin-walled glass capillaries (i.d. 0.8 mm), using a Flaming/Brown micropipette puller (Sutter Instrument Company). The ionization potential (typically 1–1.4 kV) was applied using a thin (0.368 mm) platinum wire (Alfa Aesar). The instrument was operated in ion mobility, sensitivity mode. For MS and Trap-CID experiments the SID device was tuned for "fly through" mode, so the ion beam would pass through the device without hitting the surface. A Trap gas flow rate of 4 mL/min and a Trap DC bias of 45 V are applied and the SID device is tuned to give a 1- to 5-V difference between the Trap exit and the entrance lens of the SID device and a 5- to 10-V difference between the exit lens of the SID device and the helium cell entrance.

To perform SID, operating in "Trap-SID mode" meaning the SID device is before the IM cell, the lenses on the device have to be tuned to direct the ion beam toward the surface and will depend on the system under study. The SID acceleration potential is defined as the difference between the exit of the Trap T-wave region and the surface. The SID voltage is tuned to higher or lower voltage via changing the dc bias on the Trap, which will enable the SID acceleration potential to be tuned from 10 V to 200 V. In SID mode, entrance lenses 1 and 2 are tuned to focus the beam before contact with the surface, typically 10–100 V between the two with entrance lens 1 set to 1–7 V below the exit of the Trap T-wave region while entrance lens 2 is held at approximately the same voltage as the surface. The front deflector is tuned with the top deflector 10–100 V more negative than the surface and the bottom deflector more positive than the surface. The surface is offset by 30–50 V from the helium cell dc, and the middle bottom deflector typically is 10–90 V less positive than the surface. The back deflector is tuned to focus the beam of ions after collision with the surface, the top deflector is typically 10–90 V more negative, and the bottom deflector is typically 5–90 V more negative the surface. The exit lenses are typically tuned to be 10–30 V more negative than the entrance to the helium cell. Example voltages for SID of 50 V in a Waters Synapt G2 instrument are given in *SI Appendix*, Table S2. When changing the SID acceleration potential, the Trap T-wave dc potential, entrance lens 1, and the front bottom deflector are all raised by the same potential. For SID experiments, a Trap gas flow rate of 2 mL/min is used; lowering the gas flow in this region decreases the likelihood of CID (collision with the argon trap gas) occurring alongside SID.

Preparation of the Protein Complexes. Streptavidin and neutravidin were purchased from Thermo Scientific Pierce Biotechnology, C-reactive protein and serum amyloid P were purchased from CalBioChem (EMD Biosciences, Inc.). Transthyretin, triose phosphate isomerase, insulin, cholera toxin B, phosphorylase B, D-silac acid aldolase, Con A, pyruvate kinase, hemoglobin, tryptophan synthase, urease, bovine GDH, and glutamine synthetase were all purchased from Sigma-Aldrich. All samples were analyzed at ∼10 μM complex concentration in 80 mM ammonium acetate (Sigma-Aldrich) plus 20 mM triethyl ammonium acetate (TEAA) (Sigma-Aldrich), except D-silac acid aldolase which was prepared at 160 mM AmAc and 40 mM TEAA. We used TEAA to produce "charge-reducing" conditions, which are thought to keep the complex more compact and native-like (20, 30, 31). Residual salt impurities were removed by buffer exchanging using micro-Spin 6 columns (Bio-Rad), as required.

Interfacial Analysis of Protein Complexes Using PISA. In initial SID predictions PISA, available at www.ebi.ac.uk/pdbe/pisa, was used (21). PISA can assemble protein complex structures from the Protein Data Bank (PDB) files and is used to estimate the strength of the interfaces between subunits in each complex. PISA provides the interfacial area, as well as the average number of potential hydrogen bonds and salt bridges between the subunits based upon the solved structure. From this interfacial analysis, predicted dissociation pathways were generated with the most favorable dissociation pathway being cleavage of the lowest interfacial area. The number of potential interactions broken was also noted. While this approach can be used to estimate the interface strength and hence predict the first interfaces to break, more in-depth computational analysis was required to predict the SID AE required to break the interfaces.

Computational Protein Structure Analysis and SID Prediction. ERMS plots from SID were used to determine how the individual subunits dissociated from the complex (*SI Appendix*, Figs. S8–S10). This information was then used to identify possible protein:protein interfaces that fragmented during the collision. For each of the possible fragmented interfaces, AE, which was arbitrarily defined as the acceleration energy needed to reach 10% intensity with respect to the intensity of the native complex, was determined. The experimental AEs were subsequently normalized by the number of intersubunit protein:protein contacts. For example, the homotetramer shown in *SI Appendix*, Fig. S14 dissociated into the dimers of I/II and III/IV, so there were four intersubunit protein–protein contacts (2B and 2C). Next, Rosetta's InterfaceAnalyzer (24) was used to calculate the following structural features (also normalized by number of intersubunit protein:protein contacts) of the native crystal structure complexes of the identified dissociating interfaces: change in Rosetta energy when subunits interact, change in Rosetta energy when subunits interact per area of interface, Rosetta energy of interface residues, Rosetta energy per residue for the interface, hydrophilic/hydrophobic/polar/total surface area of interface, salt bridges at interface, hydrogen bonds at interface, unsatisfied hydrogen bonds at interface, hydrogen bond Rosetta energy at interface, and number of interface residues. We used experimental AE to determine which possible quantities correlated strongly with stronger interfaces (high AE). *SI Appendix*, Fig. S11 shows correlation to AE_{exp} for the Rosetta interface ΔG (dG_separated), the hydrophobic interface surface area (dSASA_hphobic), the interface surface area (dSASA_int), and the number of interface residues (nres_int), respectively.

Even though subunit unfolding is minimized in SID compared with CID (32), precursor or subunit unfolding during the SID collision is possible. To account for this effect, RF, a measure of protein rigidity was developed, to quantify the rigidity of the subunits involved in the interface. A set of 11,060 nonredundant structures (12,591 total unique subunits) from the Protein Data Bank, obtained using PISCES (33), was analyzed. Extracting all unique subunits from complexes, we calculated the number of intramolecular SBs, HBs, and disulfide bonds (DSs), all normalized by the number of residues, using an in-house Rosetta application. The individual distributions of SBs, HBs, and DSs per residue are shown in *SI Appendix*, Fig. S15 *A–C*. Next, intrasubunit energy (E_{intra}), shown in Eq. **2**, was calculated to approximately account for the relative strengths of SBs (34), HBs (35), and DSs (36). Next, we examined the distribution of the E_{intra} values, shown in *SI Appendix*, Fig. S15*D*. Ultimately, the RF was defined to be zero if E_{intra} was more than 2 SDs below the mean, the RF was defined to be one if E_{intra} was more than 2 SDs above the mean, and linear extrapolation was used if E_{intra} was

within 2 SDs. As a consequence, the RF was bounded between zero (minimum rigidity, maximum possible unfolding during SID collision) and one (maximum rigidity, minimum possible unfolding during SID collision):

$$E_{intra} = 2.5 * SB + HB + 60 * DS. \quad [2]$$

A model was devised to predict experimental dissociation energy for given interfaces using a linear combination of the RF and the Rosetta Interface Analyzer interface parameters as shown in Eq. **1**. To optimize the model, we iteratively searched through possible combinations of parameters and optimized the weights to minimize the χ^2 between predicted and experimental AE using Python's simplex algorithm (37). The weights (w) were optimized using the training set of seven complexes and tested on a set of two complexes with known structure and four complexes for which Rosetta models exist (27).

ACKNOWLEDGMENTS. We thank Sumudu Leelananda for advice regarding interface property evaluations and Florian Busch for advice regarding additional proteins to study. We also thank Venkat Gopalan and Jikang Wu for the FraB data used in model development. We thank the Ohio Supercomputer Center for computational resources. We acknowledge financial support from the National Institutes of Health Grants R01GM113658 (to V.H.W.) (experimental SID-MS studies) and P41 GM128577 (to V.H.W. and S.L.) (computational modeling studies).

1. Uetrecht C, Barbu IM, Shoemaker GK, van Duijn E, Heck AJ (2011) Interrogating viral capsid assembly with ion mobility-mass spectrometry. *Nat Chem* 3:126–132.
2. Konijnenberg A, Butterer A, Sobott F (2013) Native ion mobility-mass spectrometry and related methods in structural biology. *Biochim Biophys Acta* 1834:1239–1256.
3. Allison TM, et al. (2015) Quantifying the stabilizing effects of protein-ligand interactions in the gas phase. *Nat Commun* 6:8551.
4. Ma X, et al. (2014) Uncovering the stoichiometry of Pyrococcus furiosus RNase P, a multi-subunit catalytic ribonucleoprotein complex, by surface-induced dissociation and ion mobility mass spectrometry. *Angew Chem Int Ed Engl* 53:11483–11487.
5. van Berkel WJH, van den Heuvel RHH, Versluis C, Heck AJR (2000) Detection of intact megaDalton protein assemblies of vanillyl-alcohol oxidase by mass spectrometry. *Protein Sci* 9:435–439.
6. Levy ED, Boeri Erba E, Robinson CV, Teichmann SA (2008) Assembly reflects evolution of protein complexes. *Nature* 453:1262–1265.
7. Marsh JA, et al. (2013) Protein complexes are under evolutionary selection to assemble via ordered pathways. *Cell* 153:461–470.
8. Beardsley RL, Jones CM, Galhena AS, Wysocki VH (2009) Noncovalent protein tetramers and pentamers with "n" charges yield monomers with n/4 and n/5 charges. *Anal Chem* 81:1347–1356.
9. Benesch JLP, Aquilina JA, Ruotolo BT, Sobott F, Robinson CV (2006) Tandem mass spectrometry reveals the quaternary organization of macromolecular assemblies. *Chem Biol* 13:597–605.
10. Hall Z, Hernández H, Marsh JA, Teichmann SA, Robinson CV (2013) The role of salt bridges, charge density, and subunit flexibility in determining disassembly routes of protein complexes. *Structure* 21:1325–1337.
11. Blackwell AE, Dodds ED, Bandarian V, Wysocki VH (2011) Revealing the quaternary structure of a heterogeneous noncovalent protein complex through surface-induced dissociation. *Anal Chem* 83:2862–2865.
12. Zhou M, Jones CM, Wysocki VH (2013) Dissecting the large noncovalent protein complex GroEL with surface-induced dissociation and ion mobility-mass spectrometry. *Anal Chem* 85:8262–8267.
13. Zhou M, Huang C, Wysocki VH (2012) Surface-induced dissociation of ion mobility-separated noncovalent complexes in a quadrupole/time-of-flight mass spectrometer. *Anal Chem* 84:6016–6023.
14. Jones CM, et al. (2006) Symmetrical gas-phase dissociation of noncovalent protein complexes via surface collisions. *J Am Chem Soc* 128:15044–15045.
15. Zhou M, Dagan S, Wysocki VH (2012) Protein subunits released by surface collisions of noncovalent complexes: Nativelike compact structures revealed by ion mobility mass spectrometry. *Angew Chem Int Ed Engl* 51:4336–4339.
16. Quintyn RS, Yan J, Wysocki VH (2015) Surface-induced dissociation of homotetramers with D2 symmetry yields their assembly pathways and characterizes the effect of ligand binding. *Chem Biol* 22:583–592.
17. Song Y, Nelp MT, Bandarian V, Wysocki VH (2015) Refining the structural model of a heterohexameric protein complex: Surface induced dissociation and ion mobility provide key connectivity and topology information. *ACS Cent Sci* 1:477–487.
18. Romano CA, et al. (2017) Biogenic manganese oxide nanoparticle formation by a multimeric multicopper oxidase Mnx. *Nat Commun* 8:746.
19. Ahnert SE, Marsh JA, Hernández H, Robinson CV, Teichmann SA (2015) Principles of assembly reveal a periodic table of protein complexes. *Science* 350:aaa2245.
20. Hall Z, Politis A, Bush MF, Smith LJ, Robinson CV (2012) Charge-state dependent compaction and dissociation of protein complexes: Insights from ion mobility and molecular dynamics. *J Am Chem Soc* 134:3429–3438.
21. Krissinel E, Henrick K (2007) Inference of macromolecular assemblies from crystalline state. *J Mol Biol* 372:774–797.
22. Quintyn RS, Zhou M, Dagan S, Finke J, Wysocki VH (2013) Ligand binding and unfolding of tryptophan synthase revealed by ion mobility-tandem mass spectrometry employing collision and surface induced dissociation. *Int J Ion Mobil Spec* 16:133–143.
23. Ma X (2014) Mass spectrometry dissociation studies of protein-protein and protein-nucleic acid complexes and 13C flux of amino acids. PhD dissertation (Ohio State Univ, Columbus, OH).
24. Lewis SM, Kuhlman BA (2011) Anchored design of protein-protein interfaces. *PLoS One* 6:e20872.
25. Harvey SR, Liu Y, Liu W, Wysocki VH, Laganowsky A (2017) Surface induced dissociation as a tool to study membrane protein complexes. *Chem Commun (Camb)* 53: 3106–3109.
26. Busch F, et al. (2018) Localization of protein complex bound ligands by surface-induced dissociation high-resolution mass spectrometry. *Anal Chem* 90:12796–12801.
27. Sahasrabuddhe A, et al. (2018) Confirmation of intersubunit connectivity and topology of designed protein complexes by native MS. *Proc Natl Acad Sci USA* 115: 1268–1273.
28. Quintyn RS, Zhou M, Yan J, Wysocki VH (2015) Surface-induced dissociation mass spectra as a tool for distinguishing different structural forms of gas-phase multimeric protein complexes. *Anal Chem* 87:11879–11886.
29. Naud C, Calas P, Blancou H, Commeyras A (2000) Synthesis of terminally perfluorinated long-chain alkanethiols, sulfides and disulfides from the corresponding halides. *J Fluor Chem* 104:173–183.
30. Pagel K, Hyung S-J, Ruotolo BT, Robinson CV (2010) Alternate dissociation pathways identified in charge-reduced protein complex ions. *Anal Chem* 82: 5363–5372.
31. Zhou M, Dagan S, Wysocki VH (2013) Impact of charge state on gas-phase behaviors of noncovalent protein complexes in collision induced dissociation and surface induced dissociation. *Analyst (Lond)* 138:1353–1362.
32. Zhou M, Wysocki VH (2014) Surface induced dissociation: Dissecting noncovalent protein complexes in the gas phase. *Acc Chem Res* 47:1010–1018.
33. Wang G, Dunbrack RL, Jr (2003) PISCES: A protein sequence culling server. *Bioinformatics* 19:1589–1591.
34. Waldburger CD, Schildbach JF, Sauer RT (1995) Are buried salt bridges important for protein stability and conformational specificity? *Nat Struct Biol* 2:122–128.
35. Steiner T (2002) The hydrogen bond in the solid state. *Angew Chem Int Ed Engl* 41:49–76.
36. Cremlyn RJW (1996) *An Introduction to Organosulfur Chemistry* (Wiley, Hoboken, NJ).
37. Kiusalaas J (2013) *Numerical Methods in Engineering with Python 3* (Cambridge Univ Press, Cambridge, UK).